# Highly amorphous titania-silica aerogels with mesopores: effect of adsorption on photocatalytic applications

István Lázár[a], József Kalmár[*b], Anca Peter[c], Anett Szilágyi[a], Enikő Győri[a], Tamás Ditrói[a]and István Fábián[a]

[a] Department of Inorganic and Analytical Chemistry, University of Debrecen, Egyetem tér 1, H-4032 Hungary

[b] MTA-DE Homogeneous Catalysis and Reaction Mechanisms Research Group, Egyetem tér 1, H-4032 Hungary

[c]Department of Chemistry and Biology, Technical University of Cluj Napoca, North University Center of Baia Mare, Baia Mare, Victoriei 76, 430122, Romania

* Author of correspondence: e-mail: kalmar.jozsef@science.unideb.hu, tel.: +36-52-512-900 / 22373

**Abstract.** Titania-silica composite aerogels with 16 – 29% Ti-content by the mass were synthesized by the sol-gel method from different Ti-precursors, and calcined at 500°C. These aerogels are highly amorphous as no crystalline $TiO_2$ phase can be detected in them by X-ray diffraction methods, and show the dominating presence of either mesopores or macropores. The incorporation of Ti into the silica structure is shown by the appearance of characteristic IR transitions of Si–O–Ti vibrations.The characteristic band-gap energies ofthe different aerogelsare estimated to be between 3.6 and 3.9 eV from UV reflection spectra. Band-gap energy decreases with decreasing pore-size. When suspended in solution,even these highly amorphous aerogels accelerate the photodegradation of salicylic acid and methylene blue compared to simple photolysis. Kinetic experiments were conducted under illumination, and also in the dark to study the adsorption of the substrates onto the suspended aerogels.We assume that the fast in-situadsorption of the organic substratesmask the suspended aerogel particles from UV photons,which reduces the rate of photocatalysis. We managed to mathematically separate the parallelprocesses of photocatalysis and adsorption, and develop a simple kinetic model to describe the reaction system.

**Keywords:**Photocatalysis; Adsorption; Titania-silica composite; Amorphous aerogel; Kinetic model

**Graphical abstract.**

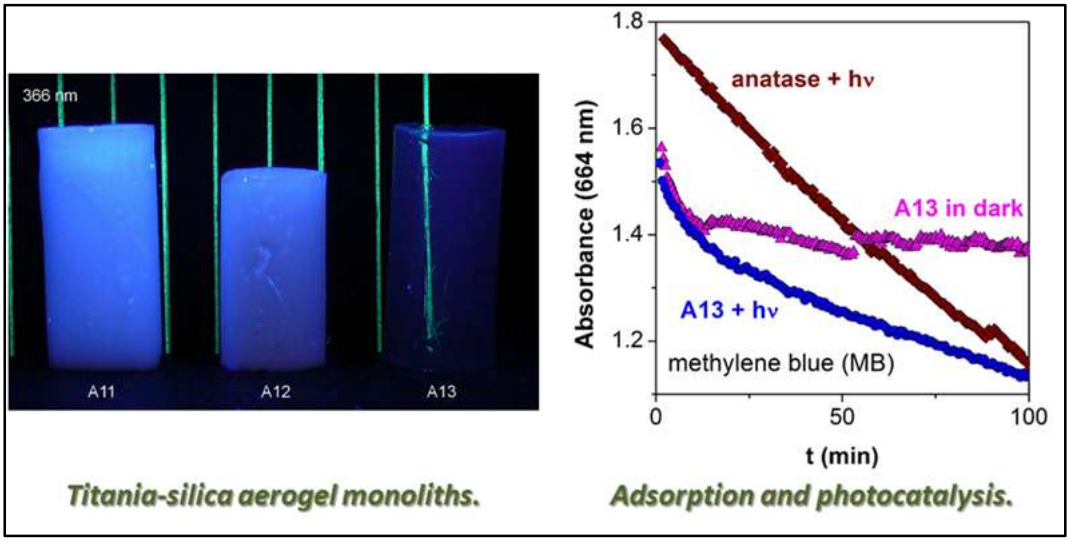


# 1. Introduction

The electronic structure of $TiO_2$ and other semiconductors (e.g. ZnO, $Fe_2O_3$, CdS, ZnS) enable them to act as sensitizers for light driven redox processes.[1] Titanium dioxide is a widely used photocatalyst due to its non-toxicity, photostability, low cost, thermal stability, biological and chemical inertness. The photocatalytic removal of a variety of organic pollutants from water and air is well studied. [2,3,4,5,6]The photocatalytic reactions of natural $TiO_2$ are driven only by UV photons and the activity of anatase is higher than that of rutile. [3,7]

The universal sol-gel processcan be appliedto prepare different, porous $TiO_2$ composites. [8,9,10]Stable sols can be obtained under acidic conditions at pH < 2 and the resulting materials usually have good photocatalytic activities. [11,12] Changing the experimental conditions and applying heat treatment influence the final composition and microstructure of the material. [13]Anatase nucleates grow first during the sol-gel process.However, calcination at higher temperatures induces a phase transformation from anatase to the thermodynamically more stable rutile. [14]The photocatalytic activity of mesoporous titania and titania-silica composites synthesized by the sol-gel method is recently a hot topic of materials research. [15,16,17,18,19,20,21,22]Pure titania aerogels were shown to be more efficient photocatalysts than titania-silica aerogels.However, it should be

emphasized, thatcomposite aerogels usually lack the structural homogeneity of $TiO_2$ and $SiO_2$ phases on the atomic scale. [23,24] In other words, some micro- or nanocrystalline $TiO_2$, usually in the form of anatase, is always present dispersed in the structure, and this crystalline phase is responsible for the photocatalytic effect.In this work we present a family of titania-silica aerogels in which no crystalline $TiO_2$can be detected by X-ray diffraction methods. Interestingly, our aerogels still display photocatalytic effects. [25,26]

The mechanism of the photodegradation reactions facilitated by $TiO_2$ and its composites have the same foundation. [27,28,29,30,31] The process is initiated by the excitation of the catalyst by $\lambda < 390$ nm light, which leads to the formation of $e^-_{CB} - h^+_{VB}$ pairs. The excitation is followed by the formation of hydroxyl radicals and superoxide radicals on the surface of the catalyst. [25]These reactive radicals readily engage in a cascade of redox reactions with organic reactants present in solution, but only near the surface of the catalyst due to their short life-time. [32]Another possible mechanism is the photosensitization of organic molecules. [33] For both processes the high adsorptivity of the catalysts is often advantageous. [34,35,36,37]It is clear however, when the active surface is masked, the photocatalytic activity vanishes. [33,38] This form of inactivation of the catalyst may be caused by the complete coverage of the active surface by the irreversible adsorption of either the reactants used in high concentrations, or by some intermediates or side products [39] of the photolysis reactions. When the active surface is covered, two fundamentalprocesses can be hindered. First, when the adsorbed molecules absorb UV light, it is possible that no photons reach the photocenters in the catalyst because of the filtering effect of the adsorbed molecules. [40] Second, even when the photocenters of the catalyst are excited, it is possible that they are sterically separated by the adsorbed moleculesfrom reactants ($O_2$, $OH^-$, organic molecules, etc.) in the bulk of the solution, thus cannot interact with them. [41,42,43]Some of the relevant studies conclude that using a high concentration of the organic substrate is detrimental in photocatalytic processes, because the complete coverage of the catalytic surface can hinder the effect of the catalysts. [33,38,40,41,42,43]

Here we clearly demonstrate,by carefully controlledand evaluated adsorption and photodegradation experiments, that the irreversible adsorption of the substrates on the surface of our mesoporous compositeaerogelsreduce theirphotocatalytic efficiencies.In addition, our results address a general problem of the heterogeneous phase photocatalysis, namely the inactivation of the catalyst by the substrate against which the catalyst is proved to be effective.

# 2. Experimental

**2.1. Materials.** Methanol (technical grade), absolutized ethanol (analytical reagent grade) and 25w% ammonia solutions (analytical reagent grade) were purchased from Molar Chemicals Kft. (Hungary). Tetramethyl orthosilicate (TMOS) (purum), acetylacetone (ReagentPlus®), titanium(IV) diisopropoxide bis(acetylacetonate) (75w% in isopropanol), titanium(IV) isopropoxide (97%), fluorescein (reagent grade), salicylic acid (analytical reagent grade, Utchim, Romania), methylene blue (reagent grade) and microcrystalline anatase ($TiO_2$, nanopowder) were obtained from Sigma-Aldrich (USA). Denatured ethyl alcohol (technical grade) was acquired from Klorid Vegyi- és Műanyagipari Zrt. (Hungary). These reagents were used without further purification.

**2.2. Aerogel preparation.** Three different titania-silica composite aerogels, labeled A11, A12 and A13, were prepared. All of these were synthesized according to the following general method. First, two solutions ("A" and "B") were prepared. In the cases of A11 and A12, solution "A" was made from tetramethyl orthosilicate(TMOS, 4.5 mL) and titanium(IV) diisopropoxide bis(acetylacetonate) dissolved in denatured ethyl alcohol (2.5 mL titanium(IV) in 5.0 mL denatured alcohol) and 400 μL acetylacetone was added to it. Solution "A" for A12 additionally contained 0.2 g fluorescein. In the case of A13, the titanium precursor was titanium(IV) isopropoxide dissolved in absolutized ethyl alcohol (1.1 mL titanium(IV) in 5.0 mL absolutized ethyl alcohol). Solution "B" contained methanol (15.0 mL), distilled water (3.75 mL) and aqueous ammonia solution (25w%, 1.00 mL) in the case of all the three composites. Solutions "A" and "B" were mixed under vigorous stirring then poured into a plastic mold and sealed. After 24 hours alcogels formed which were transferred into a perforated frame and soaked in methanol for a day. After 24 hours methanol was gradually replaced by acetone. Acetone was extracted from the gels by liquid carbon dioxide and the gels were dried under supercritical conditions[44] according to a general procedure detailed in our previous work. [45] Finally, crude aerogels were heated at 500 °C for 8 hours in a furnace under aerobic conditions to get the final calcined forms.

**2.3. Aerogel characterization.** Scanning electron microscopic (SEM) images and SEM-EDX spectra were recorded on a Hitachi S-4300 instrument (Hitachi Ltd., Tokyo, Japan) equipped with a Bruker energy dispersive X-ray spectroscope (Bruker Corporation, Billerica, MA,

USA). The monolithic aerogel samples of approximately 2 – 4 mm sizes were embedded in a low melting point alloy (Wood's metal) to decrease the possibility of accumulation of electric charge in the highly insulating aerogel samples. All fresh fracture surfaces were covered by a sputtered gold conductive layer. Typically, a 10 – 30 kV accelerating voltage was used for taking high resolution pictures.

Nitrogen gas porosimetry measurements were performed on a Quantachrome Nova 2200e surface area and porosity analyzer (Quantachrome Instruments, Boynton Beach, FL, USA) after the samples were outgassed under vacuum at 300°C for 3 hours.

IR spectra were recorded on a Jasco FT/IR 4100 spectrometer (JASCO Applied Sciences, Halifax, Canada). The aerogels were milled and pelleted into KBr for recording absorption and transmission IR spectra. The same amount of aerogel and potassium bromide was weighted in an analytical balance, thoroughly mixed and used for pelleting to record absorption spectra in each case.

UV-vis reflectance measurements of aerogelmonoliths were made by using a special accessory of the Avantes (Apeldoorn, The Netherlands) cable optic spectrophotometer of acustom built photoreactor (described in the next section). The measured sampleswere as thick as no light could pass through them. Reflectance spectra were obtained using a positioning holder, giving diffuse and specular reflectance.A standard was supplied by Avantes. The UV-vis transmission spectrum of the only transparentaerogel (A13)was recorded by the same cable optic spectrophotometer.

X-ray diffractograms were recorded by a Bruker D8 Advance X-ray Powder Diffractometer (Bruker Corporation, Billerica, MA, USA).

**2.4. Photoreactions.** The photocatalytic activities of aerogels A11, A12 and A13 were tested in 2 selected model reactions: 1) the photodegradation of salicylic acid (SA) and 2) the photodegradation of methylene blue (MB).

Salicylic acid or methylene blue was dissolved in double distilled water. A sample of one of the 3 calcined aerogels was suspended in water by the use of a Potter-Elvehjem tissue grinder and added to the solution of SA or MB. The final concentration of SA was 500 μM and that of MB was 50 μM. The final concentration of the suspended aerogel was maximum 125 μg/ml. These reaction mixtures were illuminated by high intensity UV-Vis light and the depletion of SA or MB was monitored as detailed below. Aerogel suspensions were not stored, i.e., a fresh suspension was made for each experiment. Pure SA or MB solutions were also illuminated in control experiments in the absence of an aerogel in order to study their

photolysis. Adsorption studies were carried out in the dark in solutions containing the aerogels and the organic substrates.

Two experimental setups were implemented. In one setup the experiments were carried out in a 1.0 L photoreactor equipped with a dive-in 150W medium-pressure mercury vapor lamp (Figure S1 in theSupporting Information). The lamp is axially centered in the reaction vessel and immersed into the reaction mixture. This light source is protected by a quartz tube to avoid direct contact with the aqueous solution flowing through the reactor. Both the quartz tube and the reaction vessel are double walled and were thermostated to 18 ºC with a water circulator. The reaction mixture was circulated in the reactor by anAES Laboratoire (France) peristaltic pump. The circulation rate was 0.875 L/min. Before starting illumination the aerogel suspensions were equilibrated for 10 min under constant stirring in the solution of the organic substances. After starting illumination,samples were collected from the reactor at regular intervals. The remaining amount of test substance in solution was monitored using a Perkin Elmer Lambda 35 UV-Vis Spectrophotometer (PerkinElmer, Waltham, MA, USA) at the absorption peak of 297 nm for SA and at 664 nm for MB. SA and MB concentrations were determined after centrifugation compared to external calibration solutions.

The photodegradation of MB was also studied in a different experimental setup in a custom made photoreactor, the design of which is shown in Figure S1 in theSupporting Information. This photoreactor is equipped with a laser induced xenon lamp (AvaLight-LDXE 170-1100nm; 385 mW from Avantes) as a light source for driving photoreactions. The reaction mixture was placed in a 1.00 × 1.00 cm quartz cuvette designed for spectrofluorimetry, stirred at 1000 rpm with a 8 mm Teflon coated bar and thermostated to 25 °C by a Peltier temperature controller connected to the cell holder. The light of the xenon lamp is directed through the reaction mixture by an optical cable. The photodegradation of MB was monitored on-line by spectrophotometry using a cable optic system with UV-Vis light source (AvaLight-DHc, Avantes) and a CCD detector (AvaSpec-ULS2048LTRC, Avantes). The aerogel suspensions were not pre-equilibrated in the MB solutions before starting on-line detection, thus the fast adsorption of MB could be also monitored by this technique. The light path of the photometric detection and that of the intensive illumination were perpendicular and off-planes, thus stray light could not interfere with this mode of on-line detection. A similar device is already presented in the literature. [46] On the other hand, light-scattering by the suspended aerogel lowered the signal-to-noise ratio. In spite of these difficulties, on-line detection enabled us to follow the kinetics of the photoreaction with 5 s

time resolution from as early as 30 s after mixing the aerogel suspension to the MB solution and starting illumination.

**2.5. Data treatment.** Pictures and diagrams generated by instrument controlling software are presented without manual alteration. Exceptions from this are highlighted in the narrative. When necessary, experimental data points were mathematically transformed in MS Excel. Other mathematical calculations were performed with Micromath Scientist 2.0 software (Micromath Scientific Software, St. Louis, USA).

# 3. Results

**3.1. Physical properties and appearance of aerogels.** Each synthesis yielded a 0.69 – 0.85 g calcined aerogel monolith with a density of 0.17 – 0.21 g/cm$^3$ depending on Ti-content. A11 and A12 aerogel samples (with ca. 29w% calculated Ti-content) are white non-transparent monoliths resembling to ceramics. A13 aerogel (with ca. 16 w% calculated Ti-content) on the other hand displays high transparency in the entire Vis spectral range, with only a hint of opalescence, due to Rayleigh light scattering. Photographs are presented in Figure 1 and in Figure S2 in theSupporting Information. The only difference between the syntheses of A13 and the other two aerogels was the use of a different Ti-precursor (titanium(IV) isopropoxide instead of titanium(IV) diisopropoxide bis(acetylacetonate)), besides the lower Ti-content.

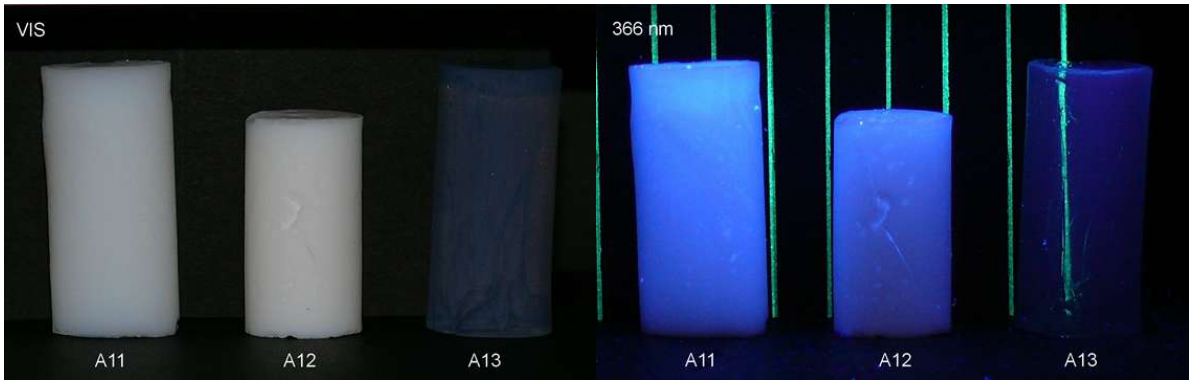


**Figure 1.** Pictures of calcined aerogel monoliths (from left to right) A11, A12 and A13 under visible light (left), as well as under 366 nm UV light (right). It should be noted that while A11 and A12 are white ceramic-like substances, A13 is transparent.

**3.2. Scanning electron microscopy and X-ray fluorescence.** SEM-images of samples A11, A12, A13 are shown in Figure 2. A11 and A12 show globular structures characteristic to silica aerogels with large macropores, the majority of which fell out of the range of nitrogen adsorption porosimetry. The structure of sample A13 is distinctive in being much more compact and tightly packed. Also, the globular building blocks are much smaller in diameter in the case of A13, and no macropores can be observed by SEM. SEM-EDX confirms the presence of Ti on the fresh fracture surfaces of all three aerogel samples as seen in the spectra shown in Figure S3 in theSupporting Information.

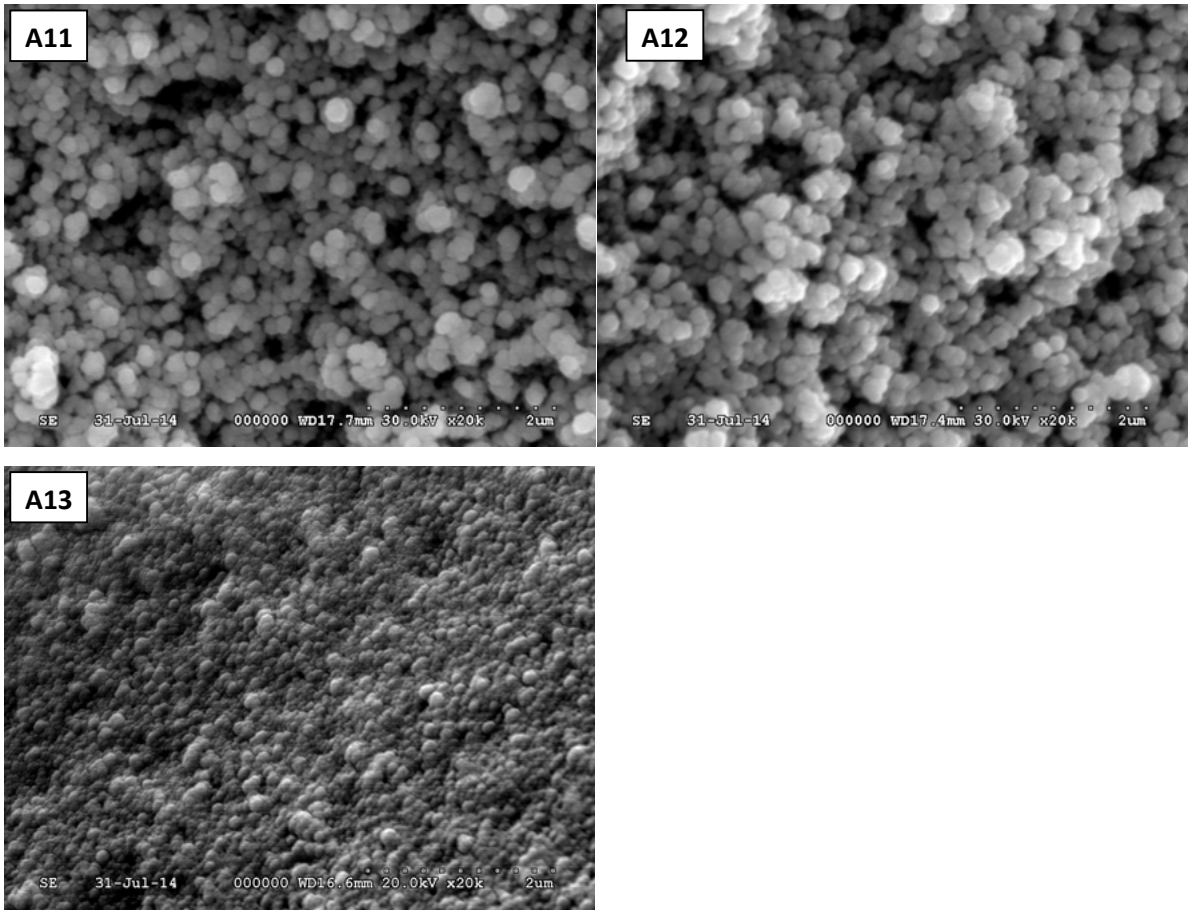


**Figure 2.** SEM micrographs of fresh fracture surfaces of calcined aerogels A11, A12 and A13.

**3.3. Nitrogen adsorption-desorption measurements.** Nitrogen adsorption-desorption isotherms of samples of A11, A12 and A13 aerogels are shown in Figure 3a. The measured data points are given in Table S1 in theSupporting Information. The isotherms describing A11 and A12 are almost identical and differ significantly from that describing A13. Adsorption

and desorption isotherms were evaluated by the BET and the BJH methods and the results are given inTable 1, Table 2 and Figure 3b. The evaluation of the same isotherms using the non-linear DFT method is presented in Table S1.The pore diameter of A13 calculated from the desorption isotherm seems larger than those of A11 and A12, regardless of the method of evaluation. In fact, as seen in the SEM images (Fig. 2), the majority of the pores of A11 and A12 are large (> 200 nm), and are over the quantification range of the used porosimetry technique. A valid and valuable conclusion is however, that A13 has considerably higher adsorption capacity and larger total specific surface area than the other two aerogels. Furthermore, A13 is the only sample of which pore size distribution is characterized by a dominating unimodal region of 10 – 20 nm pores. The contribution of larger pores are much more expressed in the case of A11 and A12 as seen in Fig. 3b.

**Table 1.** Specific surface areas and C-constants determined by the BET method from $N_2$ adsorption data.

| | **A11** | **A12** | **A13** |
|---|---|---|---|
| *Slope* | 5.891 | 7.109 | 5.260 |
| *Intercept* | 0.0505 | 0.0830 | 0.0537 |
| *Correlation coefficient* | 0.9999 | 0.9999 | 0.9999 |
| *C-constant* | 117.7 | 86.7 | 98.9 |
| *Specific surface area ($m^2/g$)* | 586.1 | 484.2 | 655.4 |

**Table 2.** Specific surface area and pore size distribution of aerogels samples calculated by the BJH method from $N_2$ adsorption and desorption physisorption data.

| | **A11** | **A12** | **A13** |
|---|---|---|---|
| *Specific surface area, adsorption ($m^2/g$)* | 389.9 | 338.4 | 475.0 |
| *Specific surface area, desorption ($m^2/g$)* | 503.6 | 419.1 | 1071 |
| *Pore diameter, adsorption (nm)* | 4.541 | 3.208 | 3.508 |
| *Pore diameter, desorption (nm)* | 3.501 | 3.184 | 14.48 |
| *Cumul. pore volume, adsorption ($cm^3/g$)* | 2.491 | 1.880 | 5.442 |
| *Cumul. pore volume, desorption ($cm^3/g$)* | 2.499 | 1.881 | 5.792 |

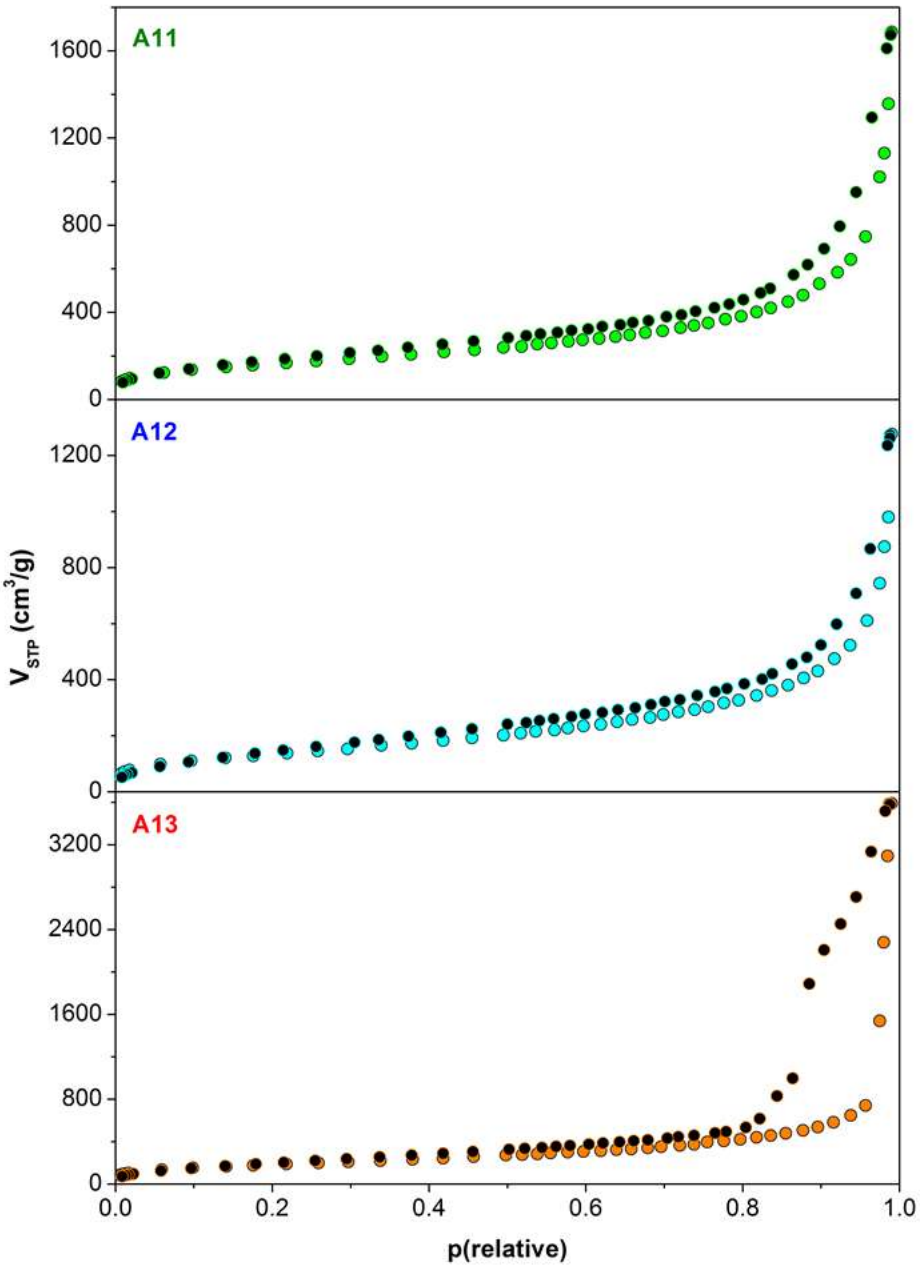


**Figure 3a.** Nitrogen adsorption-desorption isotherms of calcined aerogels A11, A12 and A13.

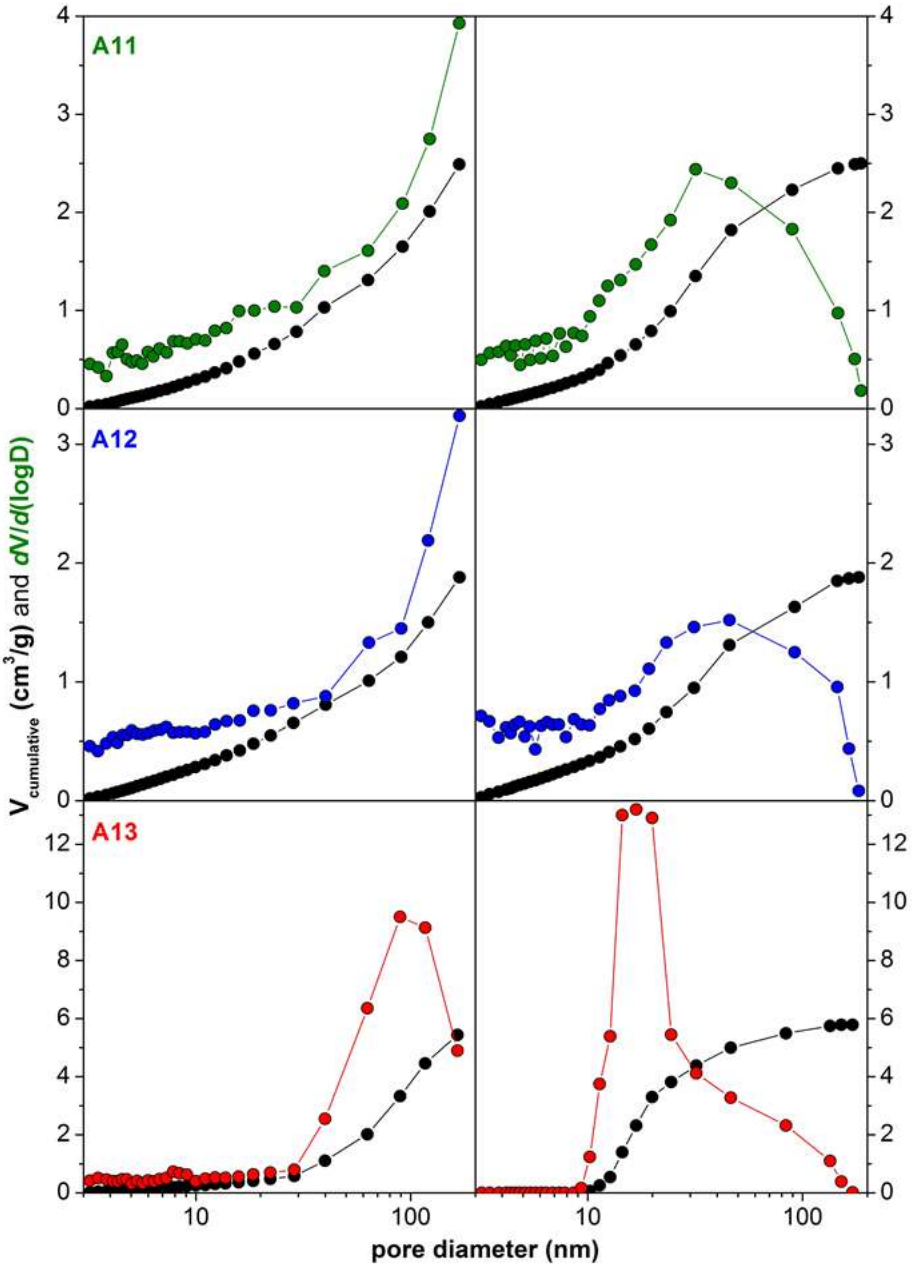


**Figure 3b.** Pore size distribution of aerogels A11, A12 and A13 calculated from $N_2$ adsorption (left) and desorption (right) isotherms, by the BJH method using 3 point floating numerical derivation. Cumulative pore volume is give in black and the derived points ($d$V/$d$logD) are colored.

**3.4. Infrared spectroscopy.** The absorption and transmission FT-IR spectra of A11, A12 and A13 aerogel samples are shown in Figure 4 and Figure S4, respectively. The bands of Si–O–Si vibrations dominate all three spectra and the peak around 1098 $cm^{-1}$ belongs to the asymmetric stretching vibration of Si–O–Si. The corresponding symmetric motion is detected at 795 $cm^{-1}$. The bands around 960 $cm^{-1}$ are due to vibrations of Ti–O–Si bonds. Bands in the region of 550 – 690 $cm^{-1}$ are usually assigned to vibrations in the $TiO_2$ bulk

phase.[26,47,48,49,50]However A11, A12 and A13 show only a minor elbow in this region which indicates the absence of a $TiO_2$ bulk phase. Following a non-linear baseline correction of the absorbance spectra (Fig. 4) we arrived to the conclusion that the intensity of all characteristic bands are similar in the three aerogel samples.

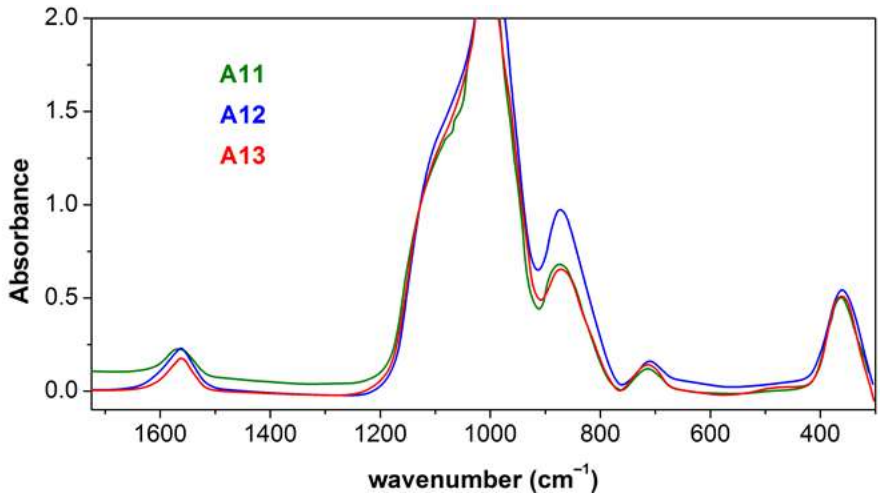


**Figure 4.** Absorption FT-IR spectra of samples from calcined aerogels A11, A12 and A1 after non-linear baseline correction.

**3.5. Powder X-ray diffraction.** No characteristic peaks of crystalline quartz or titanium dioxide forms [22] were found in any of the diffractograms of the three aerogel samples as seen in Figure S5 in theSupporting Information. This indicates the highly amorphous structure of the studied aerogels. Preliminary SAXS examinations also showedthe presence of amorphous structuresonly (see details in the Supporting Information). This finding is unexpected, because the rate of the hydrolysis reaction yielding $TiO_2$ is expected to be faster than those producing $SiO_2$ or mixed Ti–O–Si bondsduring the sol-gel process. A possible explanation is that, only small $TiO_2$ domains (> 1 nm in radius) form during the synthesis, which aredispersed in the pores. [25,26]These dispersed $TiO_2$ domains can be even conserved during calcination at 500°C. [26]The idea is further detailed in the Discussion section.

**3.6. UV-vis spectroscopy.** The reflection UV-vis spectra of A11, A12 and A13 is shown in Figure 5 together with the transmission spectrum of A13. All reflection spectra were evaluated by using the Kubelka-Munk model. The band-gap energies characteristictoourcomposite aerogelswere determined by plotting the classical $[F(R)hv]^2$

vs.*hv*functions,and calculating the abscissa intercepts of the tangents for each spectrum [51] (Figure S6 in the Supporting Information). The calculated band-gap energies are 3.90, 3.92 and 3.64 eV for A11, A12 and A13, respectively. 3.64 eV is equivalent to the energy of 340 nm photons. The transmission UV-vis spectrum of A13 has its cut-off at 340 nm, meaning that A13 in fact absorbs all photons at lower wavelengths (higher energies).

The size of the small, organized $TiO_2$ domainspresent in our aerogels can be approximated bythe comparison of the band-gap energies of the aerogels to that of bulk anatase (3.2 eV)and utilizing the theory developed by Brus. [25,52]The calculation indicates that the $TiO_2$ domains present in our calcined aerogels are actually smaller than 1 nm in radius (assuming spherical particles), and can be regarded as nanoparticles. This finding also explains the absence of XRD peaks in the case of our aerogels, as these particles are too small to yield characteristic X-ray scattering. [25]

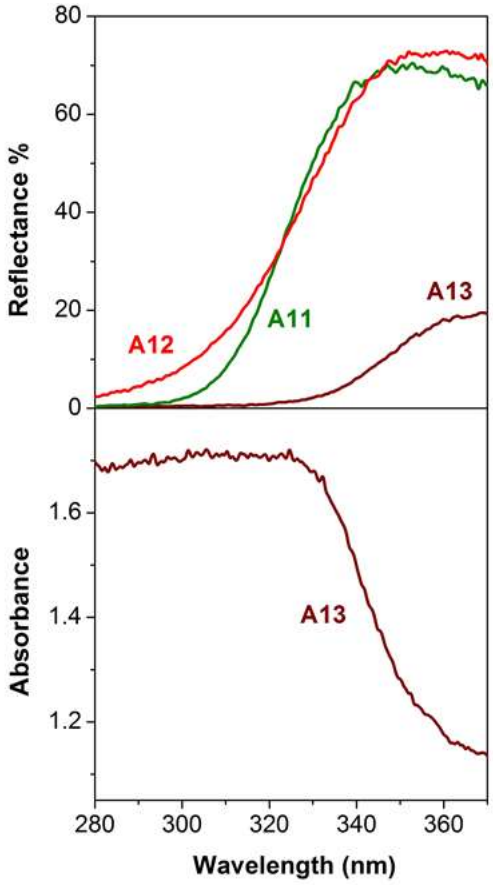


**Figure 5.**Top: UV reflection spectra of calcined aerogels A11, A12 and A13. Bottom: transmission UV spectrum of the only transparent aerogel, A13.

**3.7. Photodegradationof organic substances.** The results of the experiments conducted in the 1.0 L photoreactor are summarized in Figure 6 in the form of kinetic curves. All experiments were repeated 3 times, and the results averaged. As seen in the upper panel of Fig. 6, high intensity UV-Vis illumination degrades 12% of SA in 3 hours, while 30%, 20% and 22% of SA is degraded under the same conditions in the presence of 125 μg/ml of aerogel A11, A12 and A13, respectively. The catalytic photodegradation of SA in the presence of A13 isinitially as fast as in the presence of A11, but the former reaction considerably slows down later during the process. This is a highly unusual kinetic phenomenon, which is notdiscussedin therelevant literature.Therefore, this effect becameone of the core points of our interest, and will be detailed furtherinthe Discussion section.

Methylene blue is relatively more susceptible to photodegradation than SA: 41% of MB is degraded in the control experiment in 3 hours in the 1.0 L photoreactor, while 82%, 84% and 78% of MB is degraded under the same conditions in the presence of 125 μg/ml of A11, A12 and A13, respectively (Fig. 6bottom panel). The difference among the efficiencies of the aerogels in the MB system is thus evidently less expressed than in the SA system.

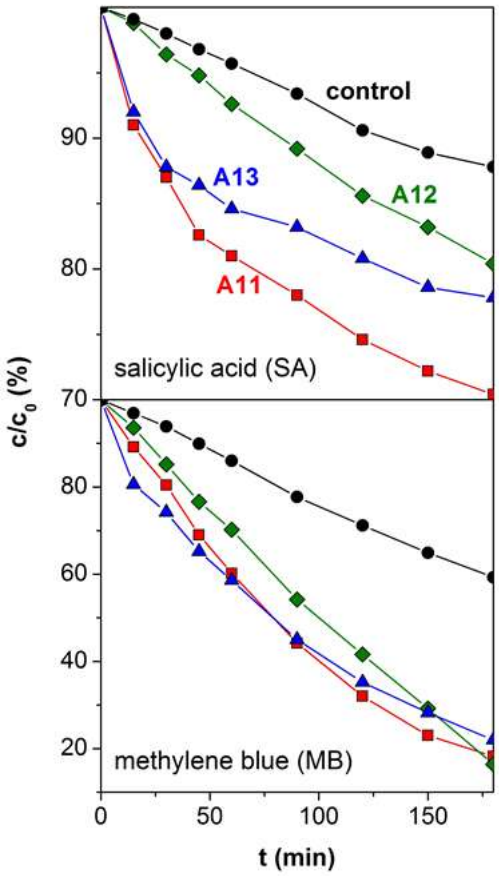


**Figure 6.** Experimental kinetic curves of the photodegradation of salicylic acid (SA, up) and methylene blue (MB, down) in the absence (●) and in the presence of one of the 3 aerogels: A11 (■), A12 (♦) and A13 (▲) suspended in solution.The kinetic curves were recorded in the 1.0 L photoreactor by off-line UV-Vis quantification. The aerogels were pre-equilibrated in the solutions of the organic substances for 10 min.All experimental points are the average of 3 parallel runs. The experimental points are connected only to guide the eye. $c_0$(SA) = 500 μM or $c_0$(MB) = 50 μM; c(aerogel) = 125 μg/ml; 18.0 ºC; 150W Hg vapor lamp.

**3.8. Adsorption of the organic substrates.**Without illumination the concentrations of SA and MB decreaseca. 2% in the presence of suspended aerogels, even after 10 min pre-equilibration. This effect was the most expressed in solutions containing A13, as seen in Figure 7, and can be obviously attributed to adsorption. It should be emphasized that while the relative amount of the adsorbed organic substances seems low, it is clear that the adsorption is fast, thus a considerable amount of the substratesare already absorbed during pre-equilibration.The real extent of adsorption is measured independently in experiments detailed in the next paragraph.

In the case of MB, the aerogel particles became visibly colored during the experiments, which means that their surface was covered by MB molecules. This coloration of the aerogel

catalyst was also clearly seen when they were recovered from the photoreactor after stopping illumination in photocatalytic experiments. When the recovered colored aerogel was re-suspended in clean water and stirred, the color was not removed. Decolorization of the aerogels could be achieved only by stirring them in 1.0 M HCl. This finding indicates that the adsorption of MB onto the surface of the aerogels is, at least to some extent, irreversible.

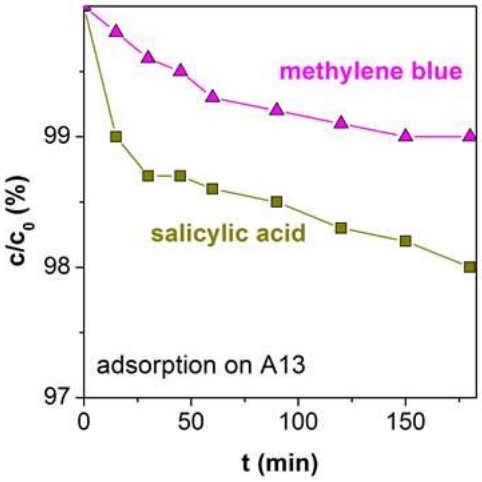


**Figure 7.** Kinetic curves of the adsorption of salicylic acid (SA, ■) and methylene blue (MB, ▲) onto suspended aerogel A13 recorded in the 1.0 L photoreactor. The systems was not illuminated during these experiments, off-line UV-Vis quantification was made. The aerogels were pre-equilibrated in the solutions of the organic substances for 10 min. All experimental points are the average of 3 parallel runs. The experimental points are connected only to guide the eye. $c_0$(SA) = 500 µM or $c_0$(MB) = 50 µM; c(A13) = 125 µg/ml; 18.0 ºC.

**3.9. Experiments in the custom built photoreactor.**The results of the experiments with MB in the custom built photoreactor are presented in Figure 8 in the form of kinetic curves. Light-scattering by the applied suspended aerogels critically lowered the signal-to-noise ratio of the on-line UV-Vis detection in the case of A11 and A12 and these results are not shown in Fig. 8 for the sake of clarity. Microcrystalline anatase was used as a reference photocatalyst to benchmark the efficiency of suspended A13 in the photodegradation of methylene blue. It is important to keep in mind that the lamp of the custom built photoreactor is much less intense than that of the 1.0 L photoreactor, therefore photoreactions are significantly slower in the former instrument. This also means that the studied photoreactions followed zeroth order kinetics for longer time, thus their rates could be easily quantified. [53,54] The ratio of the rates of the accelerated photoreactions measured under the same conditions define the relative

efficiency of different photocatalysts compared to each other. By this methodology we found that the rate of the photodegradation is 2.3 mAU/min with A13 and 5.4 mAU/min with the same mass-concentration of anatase, as seen in Fig. 8.These rates are 14.4 and 9.1 mAU/min, respectively, when corrected by the specific Ti content of the two catalysts. The uncatalyzed rate of MB photolysis was measured to be 0.04 mAU/min under the same conditions (data not shown).

An interesting feature of the kinetic traces in the presence of A13 is that the rates of MB decay are practically the same in the dark and during illumination in the first 20 minutes of the process (Fig. 8). The concentration decay becomes negligible (in the dark) and considerably slower (during illumination) at longer reaction times. The initial decay does not require the illumination of the system confirming that this phenomenon is due to the adsorption of the dye onto the suspended aerogel. Because the aerogel suspensions were not pre-equilibrated with the MB solution, a better approximation can be given for the absorbed amount of MB based on this experiment. The initial fast decay of the kinetic curves accounts for ca. 0.2 AU, which is 13% of the initial absorbance of MB (1.58 AU). This means, thatca. 3.8 μmol MB is adsorbed by 57.4 mg A13 aerogel, which is a considerable amount. It is also clearly seen, that the adsorption process is practically complete in 15 min, which explains the lower observed effect after the aerogel was pre-equilibrated in the 1.0 L photoreactor for 10 min (cf. Fig. 7).We tried to conduct similar on-line fast adsorption measurements with salicylic acid, but our detector signal was too noisy in the UV region (where SA absorbs), because of light scattering. We assume however, that the negatively charged SA adsorbs slower to the surface of the titania-silica aerogels, which can account for the significant drop of SA concentration measured even after 10 min pre-equilibration in the 1.0 L photoreactor in the dark (cf. Fig. 7).

It should be noted, that the applied SA concentration was 500 μM in the 1.0 L photoreactor, 10-times higher than that of MB.Therefore, the absolute amount of adsorbed SA is higher than that of MB, lowtenths of micromoles per milligram A13, as verified by batch adsorption experiments (180 min equilibration, data not shown).

Adsorption processes as fast as the above described can compete in rate with photocatalytic reactions. Usually no effort is invested to mathematically separate these two processesduring data evaluation, which could lead to erroneous conclusions regarding the photocatalytic efficiency of materials which are also good adsorbents. In the Discussion section we propose anoveldata evaluation method based on the principles of reaction kinetics to computationally separate the competing processes, and show the effect of adsorption.

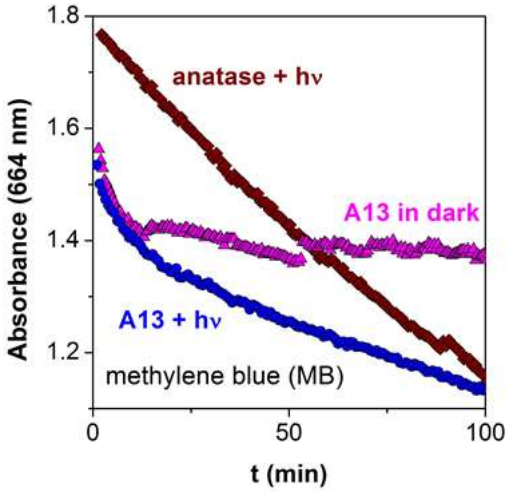


**Figure 8.** Experimental kinetic curves of the photodegradation of methylene blue (MB) in the presence of microcrystalline anatase and suspended aerogel A13 recorded in the custom built photoreactor. All kinetic curves were recorded by on-line UV-Vis spectrophotometry at 664 nm and only every fifth experimental point is shown for clarity. The slope of the kinetic curves measured from 35 min to 85 min is $-(5.4\pm0.1)\times10^{-3}$ AU/min in the presence of anatase and $-(2.32\pm0.05)\times10^{-3}$ AU/min in the presence of A13. A control experiment is also shown where suspended A13 was mixed to MB in the dark. A faster process can be seen in the first 20 min of the 2 kinetic curves in the presence of A13. This process is attributed to the adsorption of MB onto the suspended aerogel. $c_0$(MB) = 29.1 μM; c(Anatase) = 57.1 μg/ml; c(A13) = 57.4 μg/ml; 25.0 ºC; laser induced Xenon lamp.

# 4. Discussion

**4.1. Structure of the aerogels.** All the three studied aerogels have unique structure in the sense that no crystalline anatase phase could be detected in them by X-ray diffraction methods. Even the IR bands usually assigned to the $TiO_2$ bulk phase in titania-silica composite aerogels are weak in their recorded IR spectra.Earlier reports indicate that titania-silica aerogels with different microstructures can be synthesizedby varying the conditions of the sol-gel process, but these composites always contain crystalline $TiO_2$ to some extent. [8,14,19,55,56] A possible explanation for the absence of diffraction peaks and IR bands in titania-silica composites prepared by the sol-gel method is given by Zeleňák et. al. [26] These authors characterized titania-silica composites (with maximum 30w% Ti content) calcined at temperatures lower than 650 °C to contain mainly incorporated Ti in the form of Ti–O–Si, and no bulk $TiO_2$.They propose the presence of separated $TiO_2$nanoparticles [25] as efficient centers for photocatalysis builtinto the walls of the mesopores. We accept this theory to be

valid in our case as well, asit is supported by the measured considerable increase of the band-gap energies of our composite aerogels compared to bulk anatase.

Based on the appearance, $N_2$ adsorption properties and SEM micrograph it is clear that the structure and thus the physico-chemical properties of calcined aerogel A13 are remarkably different from those of A11 and A12. The intensity of the IR absorption peak around 960 $cm^{-1}$ describing Ti–O–Si bonds is only slightly smaller in the case of A13 not reflecting the different chemical composition of this aerogel, i.e., its lower specific Ti-content (A13: ca. 16w%; A11 and A12:ca. 29w%). Besides chemical composition, the porosity of A13 is also generally different from that of the other two composites. Nitrogen adsorption-desorption experiments proved that A13 is the only aerogel which displays a dominating relatively narrow distribution of pores around 10 – 20 nm within the studied 3 – 195 nm diameter range. This is in accordance with the highly ordered structure of smaller characteristic globular building blocks seen in the SEM micrograph of A13. Furthermore, the highest total pore volume and specific surface area predicts that A13 is the best adsorbent among the studied aerogels. It is worth noting that A11 and A12 clearly display pores significantly larger than 200 nm as seen in their SEM micrographs (Fig. 2). These pores however cannot be quantitatively characterized by the applied porosimetry method.We propose that the transparency of calcined aerogel A13 is cooperatively caused by its characteristic porosity and lower Ti-content.The higher Ti content of A11 and A12 causes a change in porosity, which in turn alters the light-scattering properties of the aerogels.

Porous materials containingoverlapping $TiO_2$ domainsare usually better photocatalysts than those containingwell-separated nano-scale photocenters, because the operation of quantum effects increase the band gap energy of $TiO_2$ in the latter case. [25,33,34]Normally, photoactive $TiO_2$nanoparticles are more separatedin composites with lower Ti content, andbecome more agglomerated and overlapping with increasing Ti content and with increasing calcination temperature. [25,26] We found that the estimated band-gap energy of A13islower by almost 0.3 eV than those of A11 and A12, as shown in the Results section. This could mean that the $TiO_2$ domains are more overlapping in A13. A13 has the finest and most ordered microstructure(with small spherical building blocks and small pores) among our aerogels. We assume, that this ordered microstructure could lead to the formation of larger $TiO_2$ domains during the synthesis, which can be caused by the use of the different Ti-precursor (titanium(IV) isopropoxide), besides the lower Ti-content.

Obviously,its lower band-gap energy, higher transparency and higher specific surface area makes A13 to be comparable in photocatalytic efficiency to A11 and A12.

**4.2. Photodegradation of organic substances.**Our experimental results prove that all three calcined aerogels accelerate the photodegradation of both salicylic acid (SA) and methylene blue (MB) when suspended in their solutions. We benchmarked A13against anatase, and found, that this composite aerogelis only aslightly better photocatalystthan anatase when contrasted to the weight of Ti present in the materials. However,the adsorption of the substrate may affect its catalytic efficiency, as detailed in the next paragraph.The comparison of our catalyststo other aerogels presented in the literature is problematic, because of the differences in the applied light-sources and experimental conditions. However, we foundthat the catalytic efficiencies and reaction ratesreportedpreviously with compositeaerogels [10,22,25,50] are very similarto our results.

The experimental kinetic curves obtained in the 1.0 L photoreactor have intriguing shape. Specifically, a fast drop in reaction rate is seen during the photodegradation of SA when it is catalyzed by A13 (cf. Fig. 6 left panel). This kinetic curve cannot be simulated by taking into account only the depletion of SA in unhindered parallel photoreactions, i.e. using the widely accepted kinetic approximations (Langmuir-Hinshelwood model) [25,33,43] for the catalyzed process, and the photochemical model [53,54,57] for the uncatalyzed process. In other words, the amount of SA consumed and the drop of reaction rate cannot be described by two parallel pseudo-first-order photoreactions. [58] (results not shown)

To account for the significant drop in reaction rate, we constructed an elaborate kinetic model [37,39] step by step as follows. 1) The rate of the non-catalyzed photolysisof SA is independently given by the control experiment conducted in the absence of A13. 2) We assume that the considerable extent of the in-situ fast adsorption of the substrate (detected also in the absence of illumination) leads to the poisoning of A13,because most of the UV photons will be absorbedby the organic layer,thus cannot reach the $TiO_2$ photocenters. 3) As long as the previous adsorption process is far from completion the suspended aerogel participates in the photodegradation of SA and catalyzes it. When the surface of A13 is extensively covered, it is no longer active and SA will degrade only by the uncatalyzed rate. This phenomenon is clearly seen in Fig. 6 and 9, as the kinetic curves of the catalyzed and uncatalyzed processes become parallel after 50 min. The proposed kinetic model is summarized in Scheme 1.It is evident that, for efficient photocatalysis in step 3), SA has to come into close contact with the surface of A13, e.g. in the form of reversible adsorption. Thus, we presume that the in-situ poisoning of the suspended aerogel takes place only in a parallel fast process, i.e. the persistent adsorption of SA and the masking of the catalytic

centers in step 2). Further, reaction kinetics based considerations are given in the Supporting Information.

**1)** SA $\xrightarrow{h\nu}$ Products $\quad k_1$

**2)** SA + $A13_{surface} \xrightarrow{ads.}$ (masked surface) $\quad k_2$

**3)** SA + $A13_{surface} \xrightarrow{h\nu}$ Products + $A13_{surface}$ $\quad k_3$

$$\frac{d[\mathrm{SA}]}{dt} = -k_1\left(1 - 10^{-El[\mathrm{SA}]}\right) - k_2[\mathrm{SA}][\mathrm{A13surf}] - k_3[\mathrm{SA}][\mathrm{A13surf}] \mathrm{eq.1}$$

$$\frac{d[\mathrm{Prod}]}{dt} = +k_1\left(1 - 10^{-El[\mathrm{SA}]}\right) + k_3[\mathrm{SA}][\mathrm{A13surf}] \quad \mathrm{eq.2}$$

$$\frac{d[\mathrm{A13surf}]}{dt} = -k_2[\mathrm{SA}][\mathrm{A13surf}] \mathrm{eq.3}$$

**Scheme 1.** Kinetic model for the accelerated photodegradation of salicylic acid (SA) in the presence of suspended aerogel A13. The symbol *hv* indicates that photons take part in a reaction step. The first process is the uncatalyzed photodegradation of SA. The second process is the irreversible adsorption of SA onto the surface of A13 which in-situ poisons the catalyst. The third process is the catalyzed photodegradation of SA. The 3 reaction steps are characterized by rate constants $k_1$, $k_2$, $k_3$, respectively. *E* is the molar absorption coefficient of SA and *l* is the optical pathlength.

The results of the mathematic simulation based on reactions 1) to 3) of Scheme 1 are shown in Figure 9. All 3 kinetic curves (adsorption, photolysis, photocatalysis) recorded in the experiments with SA were taken into account simultaneously during the calculation. We ensured by using this approach, that all chemical effects were incorporated with the same weight into the mathematical procedure. Further details on the calculation are given in theSupporting Information. An extrapolation on the course of the catalyzed photodegradation in the absence of process 2) (i.e. without the poisoning of the catalyst) is also given in Fig. 9. The simulation based on the model of Scheme 1 satisfactorily describes the experimental data, i.e. the three independent kinetic curves (adsorption, photolysis, and photocatalysis).

The approach utilized in the case of SA and A13 can be used without modification to describe the reaction system of methylene blue and A13 (cf. Fig. 6, right panel). The results of the mathematical simulation are in good agreement with measured data in the case of MB as well, as seen in Fig. 9 right panel.

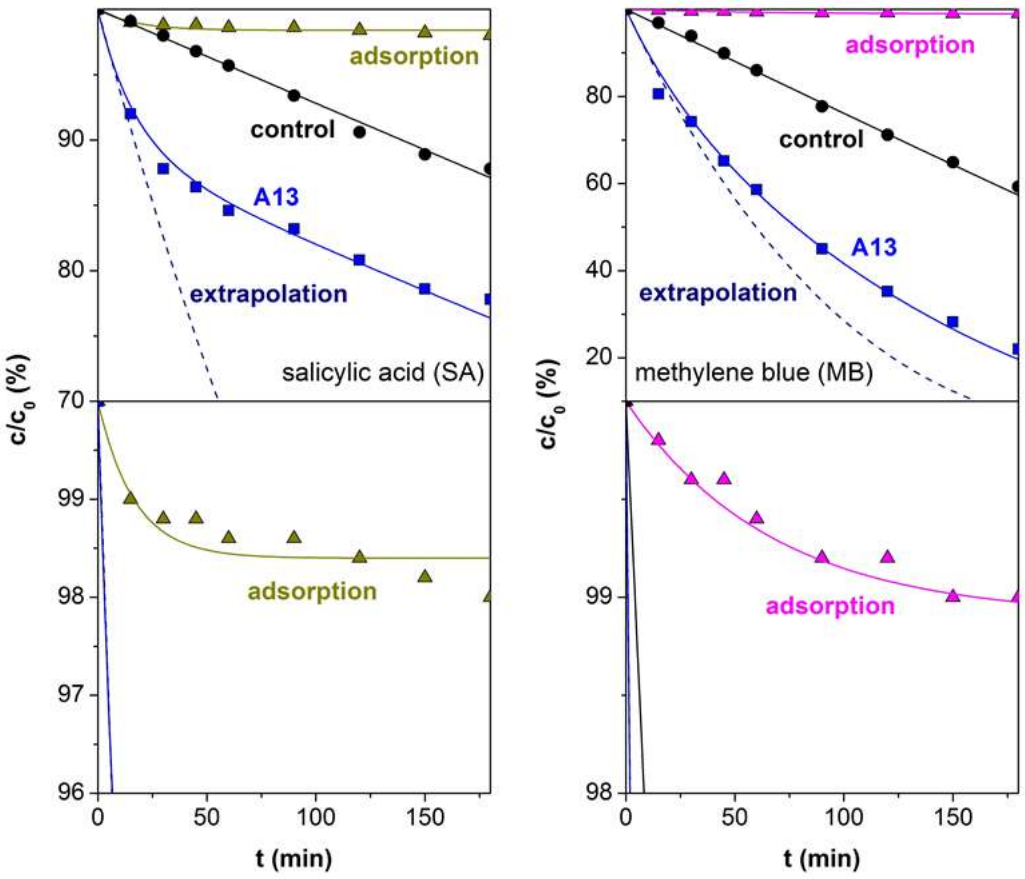


**Figure 9.** Experimental kinetic curves of the photodegradation of salicylic acid (SA, left panel) and methylene blue (MB, right panel) in the absence (●) and in the presence of suspended aerogel A13 (■). The bottom figures were magnified from the top ones and show the same adsorption data set as Fig.7. All kinetic curves were recorded in the 1.0 L photoreactor by off-line UV-Vis quantification. Continuous lines are the results of mathematical simulation based on the kinetic model of Scheme 1. All kinetic curves of a given reaction system (either with SA or MB) were calculated simultaneously. Dashed lines represent extrapolated kinetic curves calculated without taking into account the in-situ poisoning of the suspended aerogel. $c_0$(SA) = 500 μM or $c_0$(MB) = 50 μM; c(aerogel) = 125 μg/ml; 18.0 ºC; 150W Hg vapor lamp.

As a summary, we can state that our results suggest that the efficiencies of the suspended aerogels are greatly affected by the fast adsorption of the test substances onto their surfaces. It is evident that the adsorption of the organic substrates to be degraded is required

for efficient photocatalysis, but fast, persistent adsorption can also poison the catalyst,as detailed in the Introduction. [33,38,40,41,42,43] We assume that when SA or MB adsorbs to the surface of the suspended aerogel particles they lower the number of UV photons reaching the catalytic centers, because these organic substances readily absorb UV light. Furthermore in the case of an irreversible adsorption, the steric accessibility of the surface to other reactants can be also hindered. The experimental evidence for this assumption is the unexpected considerable decrease of the rate of the catalytic photodegradation which is simultaneous with the completion of the adsorption process (cf. Fig. 6, 7 and 9). Furthermore, we showed that the adsorption of MBto aerogel A13 is fast (cf. Fig. 8), and at least partially irreversible, which are prerequisites for the effective masking of the surface.One way of validating our assumptions was the mathematical simulation of the kinetic curves recorded in the presence of suspended A13 with the model of Scheme 1. Obviously,A13 was chosen because it has the largest specific surface area and adsorptive capacity, thus the deceleration of the catalytic reaction rate is the most expressed in the case of A13 (cf. Fig. 6, 7 and 9).

It is interesting to compare the photoreactions of SA and MB in the presence of A13. The catalytic efficiency of A13 is ruinedto a significantly higher extent during the photodegradation of SA, than in the system with MB. This effect is clearly seen in Fig. 9 when we compare the extrapolated kinetic curves calculated by excluding the poisoning of the catalyst (dashed lines). We assume, that the coverage of the surface of A13 by MB is practically complete during the 10 min pre-equilibration, thus the effect of adsorptionis less expressedin the longer time scale. On the other hand, SA adsorbs slower to A13, therefore its effect on the kinetics of photocatalysis can be conveniently detected by the slower off-line quantification method.

In spite of the similarity of A11 and A12, the latter proved to be a significantly worse catalyst for the photodegradation of SA (cf. Fig. 6 left panel). We presume that entrapped residues of fluorescein or its thermal decomposition products present in A12 might act as internal light filters, thus decreasing the amount of photons absorbed by the photocenters and decreasing catalytic efficiency.

# 5. Conclusions

Titania-silica composite aerogels were synthesized by the general sol-gel method from different Ti-precursors. The structure of these compounds are highly amorphous after calcination at 500 °C and the resulting monoliths are built up from small and partly overlapping globules characteristic to silica aerogels. The crystalline $TiO_2$ bulk phase is absent from these composites.Instead, we assume that $TiO_2$ nanoparticles aredispersed in the silicastructure. [25,26] Thepacking of globules, pore size distribution, specific surface area and even the optical properties can be tuned by adjusting the Ti-content and choosing theTi-precursor. It was shown that all our titania-silica aerogels suspended in solution catalyze the photodegradation of salicylic acid and methylene blue under high intensity UV-Vis illumination. The aerogel with the lowest Ti-content and highest porosity (A13) is as efficient in accelerating the photodegradation reactions as the other studied aerogels, probably because its finer microstructure enables the interaction of its $TiO_2$nanocenters, lowering the measured band-gap energy.

While a high specific surface area is usually advantageous with respect to catalytic activity, we found that our organic test substances rapidly adsorb to the surface of these porous materials and, surprisingly, poison the suspended aerogel catalysts during the photodegradation reactions. We attribute this phenomenon to the UV-filter effect of the absorbed substances. As expected, this side effectis the most pronounced in the case of the aerogel with the highest specific surface area (A13). We managed to kinetically separate the adsorption and the catalytic processes during data evaluation. A simple kinetic model incorporating the previously described detrimental adsorption was developed to simulate the experimental kinetic curves of the photoreactions.

# Acknowledgement

We are grateful to Lajos Daróczy (University of Debrecen) for the electron microscopy measurements and Attila Kiss (University of Debrecen) for the IR measurements. The help of Márton Benke (University of Miskolc) in the powder X-ray measurements and the assistance of Zsolt Erdei (University of Debrecen) with the custom built photoreactor are greatly acknowledged. We greatly appreciate the SAXS results kindly supplied by Ádám Juhász and

Imre Dékány (University of Szeged). The authors thank the Hungarian Science Foundation (OTKA: NK 105156)and the University of Debrecen (RH/751/2015) for financial support. The research was also supported by the EU and co-financed by the European Social Fund under the projects ENVIKUT (TAMOP-4.2.2.A-11/1/KONV-2012-0043).

## Appendix A. Supplementary material

The description of the photoreactors, pictures of calcined aerogels, powder X-ray diffractograms, transmission infrared spectra, X-ray fluorescence spectra, and details on the kinetic calculations can be found in electronic Supporting Information.

## References

[1] M. R. Hoffmann, S. T. Martin, W. Choi, D. W. Bahnemann, Environmental applications of semiconductor photocatalysis, Chem. Rev. 95 (1995) 69-96.

[2] B. Sun, E. P. Reddy, P. G. Smirniotis, Effect of the $Cr^{6+}$ concentration in Cr-incorporated $TiO_2$-loaded MCM-41 catalysts for visible light photocatalysis,Appl. Catal. B: Environ. 57 (2005) 139-149.

[3] Y. Zhang, W. Rong, Y. Fu, X. Ma, Photocatalytic degradation of Poly(Vinyl Alcohol) on $Pt/TiO_2$ with Fenton Reagent, J. Polym. Environ. 19 (2011) 966-970.

[4] A. Fujishima, X. Zhang, Titanium dioxide photocatalysis: present situation and future approaches, Compt. Rend. Chim. 9 (2006) 750-760.

[5] H. M. Coleman, E. J. Routledge, J. P. Sumpter, B. R. Eggins, J. A. Byrne, Rapid loss of estrogenecity of steroid estrogens by UVA photolysis and and photocatalysis over an immobilised titanium dioxide catalyst,Water Res. 38 (2004) 3233-3240.

[6] K. Sato, T. Hirakawa, A. Komano, S. Kishi, C. K. Nishimoto, N. Mera, M. Kugishima, T. Sano, H. Ichinose, N. Negishi, Y. Seto, K. Takeuchi, Titanium dioxide photocatalysis to decompose isopropyl methylphosponofluoridate (GB) in gas phase, Appl. Catal. B: Environ. 106 (2011) 316-322.

[7] F. Adam, J. N. Appaturi, Z. Khanam, R. Thankappan, M. A. M. Nawi, Utilization of tin and titanium incorporated rice husk silica nanocomposite as photocatalyst and adsorbent for the removal of methylene blue in aqueous medium,Appl. Surf. Sci. 264 (2013) 718-726.

[8] L. K. Campbell, B. K. Na, E. I. Ko, Synthesis and characterization of titania aerogels, Chem. Mater. 4 (1992) 1329-1333.

[9] G. J. D. A. Soler-Illia, C. Sanchez, B. Lebeau, J. Patarin, Chemical strategies to design textured materials: from microporous and mesoporous oxides to nanonetworks and hierarchical structures, Chem. Rev. 102 (2002) 4093-4138.

[10] A. Sachse, V. Hulea, K. L. Kostov, E. Belamiea, B. Alonso, Improved silica–titania catalysts by chitin biotemplating,Catal. Sci. Tech. 5 (2015) 415-427.

[11] L. Luo, A. T. Cooper, M. Fan, Preparation and application of nanoglued binary titania–silica aerogel, J. Hazard. Mater. 161 (2009) 175-182.

[12] S. Rasalingam, R. Peng, R. T. Koodali, Removal of hazardous pollutants from wastewaters: applications of $TiO_2$-$SiO_2$ mixed oxide materials, J. Nanomater. 10 (2014) DOI: 10.1155/2014/617405

[13] N. Yao, S. Cao, K. L. Yeung, Mesoporous $TiO_2$–$SiO_2$ aerogels with hierarchal pore structures, Micropor. Mesopor. Mat. 117 (2009) 570-579.

[14] C. Su, B. Y. Hong, C. M. Tseng, Sol-gel preparation and photocatalysis of titanium-dioxide,Catal. Today 96 (2004) 119-126.

[15] S. Murali, S. P. Lee, D. P. Birnie III, The importance of silica morphology in silica-titania composites with dye sensitized solar functionality, Thin Solid Films 537 (2013) 80-84.

[16] K. Li, T. Chen, L. Yan, Y. Dai, Z. Huang, J. Xiong, D. Song, Y. Lv, Z. Zeng, Design of graphene and silica co-doped titania composites with ordered mesostructure and their simulated sunlight photocatalytic performance towards atrazine degradation, Colloids Surf. A 422 (2013) 90-99.

[17] C. Akly, P. A. Chadik, D. W. Mazyck, Photocatalysis of gas-phase toluene using silica-titania composites: Performance of a novel catalyst immobilization technique suitable for large-scale applications, Appl. Catal. B: Environ. 99 (2010) 329-335.

[18] J. L. Coutts, L. H. Levine, J. T. Richards, D. W. Mazyck, The effect of photon source on heterogeneous photocatalytic oxidation of ethanol by a silica–titania composite, J. Photochem. Photobiol. A 225 (2011) 58-64.

[19] A. Hilonga, J. K. Kim, P.B. Sarawade, H. T. Kim, Rapid synthesis of homogeneous titania-silica composite with high-BET surface area, Powder Technol. 199 (2010) 284-288.

[20] H. E. Byrne, D. W. Mazyck, Removal of trace level aqueous mercury by adsorption and phtocatalysis on silica-titania composites, J. Hazard. Mater. 170 (2009) 915-919.

[21] E. Pitoniak, C. Y. Wu, D. Londeree, D. Mazyck, J. C. Bonzongo, K. Powers, W. Sigmund, Nanostructured silica-gel doped with $TiO_2$ for mercury vapor control, J. Nanopart. Res. 5 (2003) 281-292.

[22] S. V. Ingale, P. U. Sastry, P. B. Wagh, A. K. Tripathi, R. Rao, R. Tewari, P. T. Rao, R. P. Patel, A. K. Tyagi, S. C. Gupta, Synthesis and micro structural investigations of titania–silica nano composite aerogels, Mater. Chem. Phys. 135 (2012) 497-502.

[23] B. Malinowska, J. Walendziewski, D. Robert, J. V. Weber, M. Stolarski, The study of photocatalytic activities of titania and titania-silica aerogels, Appl. Catal. B: Environ. 46 (2003) 441-451.

[24] H. Zhang, X. Quan, S. Chen, H. Zhao, Y. Zhao, The removal of sodium dodecylbenzene sulfonate surfactant from water using silica/titania nanorods/nanotubes composite membrane with photocatalytic capability, Appl. Surf. Sci. 252 (2006) 8598-8604.

[25] a) C. Anderson, A. J. Bard, An improved photocatalyst of $TiO_2/SiO_2$ prepared by a sol-gel synthesis, J. Phys. Chem. 99(24), 1995, , 9882-9885.
b) C. Anderson, A. J. Bard, Improved photocatalytic activity and characterization of mixed $TiO_2/SiO_2$ and $TiO_2/Al_2O_3$ materials, J. Phys. Chem. B 101 (1997) 2611-2616.

[26] V. Zelenak, V. Hornebecq S. Mornet, O. Schäf, P. Llewellyn, Mesoporous silica modified with titania: Structure and thermal stability,Chem. Mater. 18 (2006) 3184-3191.

[27] J. Bandara, J. A. Mielczarski, J. Kiwi, Molecular mechanism of surface recognition. Azo dyes degradation on Fe, Ti and Al oxides through metal sulfonate complexes, Langmuir 15 (1999) 7670-7679.

[28] H. Zhan, H. Tian, Photocatalytic degradation of acid azo dyes in aqueous $TiO_2$ suspension I. The effect of substituents, Dyes Pigments 37 (1998) 231-239.

[29] A. B. Prevot, C. Baiocchi, M. C. Brussino, E. Pramauro, P. Savarino, V. Augugliaro, G. Marcí, L. Palmisano, Photocatalytic degradation of acid blue 80 in aqueous solutions containing $TiO_2$ suspensions, Environ. Sci. Technol. 35 (2001) 971-976.

[30] N. Daneshvar, D. Salari, A. R. Khataee, Photocatalytic degradation of azo dye acid red 14 in water: investigation of the effect of operational parameters, J. Photochem. Photobiol. A 157 (2003) 111-116.

[31] K. Tanaka, K. Padermpole, T. Hisanaga, Photocatalytic degradation of commercial azo dyes, Water Res. 34 (2000) 327-333.

[32] C. Minero, F. Catozzo, E. Pelizzetti, Role of adsorption in photocatalyzed reactions of organic molecules in aqueous titania suspensions, Langmuir 8 (1992) 481-486.

[33] I. K. Konstantinou, T. A. Albanis, $TiO_2$-assisted photocatalytic degradation of azo dyes in aqueous solution: kinetic and mechanistic investigations: a review, Appl. Catal. B: Environ. 49 (2004) 1-14.

[34] L. He, N. Du, C. Wang, X. Chen, W. Zhang, A facile synthesis of graphene-supported mesoporous $TiO_2$ hybrid sheets with uniform coverage and controllable pore diameters, Micropor. Mesopor. Mat. 206 (2015) 95-101.

[35] A. Molinari, L. Samiolo, R. Amadelli, EPR spin trapping evidence of radical intermediates in the photo-reduction of bicarbonate/$CO_2$ in $TiO_2$ aqueous suspensions, Photochem. Photobiol. Sci. (2015) DOI: 10.1039/C4PP00467A

[36] H. S. Kibombo, R. Peng, S. Rasalingam, R. T. Koodali, Versatility of heterogeneous photocatalysis: synthetic methodologies epitomizing the role of silica support in TiO2 based mixed oxides, Catal. Sci. Tech. 2 (2012) 1737-1766.

[37] Y. Li, C. Liu, P. Xu, M. Li, M. Zen, S. Tang, Controlled fabrication of ordered mesoporous titania/carbon fiber composites with high photoactivity: Synergistic relationship between surface adsorption and photocatalysis, Chem. Eng. J. 243 (2014) 108-116.

[38] K. Gude, V. M. Gun'ko, Adsorption and photocatalytic decomposition of methylene blue on surface modified silica and silica-titania, J. P. Blitz, Colloids Surf. A 325 (2008) 17-20.

[39] S. Dutta, S. A. Parsons, C. Bhattacharjee, P. Jarvis, S. Datta, S. Bandyopadhyay, Kinetic study of adsorption and photo-decolorization of Reactive Red 198 on $TiO_2$ surface, Chem. Eng. J. 155 (2009) 674-679.

[40] M. Saquib, M. Muneer, $TiO_2$-mediated photocatalytic degradation of a triphenylmethane dye (gentian violet), in aqueous suspensions, Dyes Pigments 56 (2003) 37-49.

[41] C. M. So, M. Y. Cheng, J. C. Yu, P. K. Wong, Degradation of azo dye Procion Red MX-5B by photocatalytic oxidation, Chemosphere 46 (2002) 905-912.

[42] S. Sakthivel, B. Neppolian, M. V. Shankar, B. Arabindoo, M. Palanichamy, V. Murugesan, Solar photocatalytic degradation of azo dye: comparison of photocatalytic efficiency of ZnO and $TiO_2$, Sol. Energ. Mater. Sol. C. 77 (2003) 65-82.

[43] S. Brosillon, L. Lhomme, C. Vallet, A. Bouzaza, D. Wolbert, Gas phase photocatalysis and liquid phase photocatalysis: interdependence and influence of substrate concentration and photon flow on degradation reaction kinetics, Appl. Catal. B: Environ. 78 (2008) 232-241.

[44] S. Smitha, P. Shajesh, P. R. Aravind, S. R. Kumar, P. K. Pillai, K. G. K. Warrier, Effect of aging time and concentration of aging solution on the porosity characteristics of subcritically dried silica aerogels, Micropor. Mesopor. Mat. 91 (2006) 286-292.

[45] I. Lázár, H. F. Bereczki, S. Manó, L. Daróczi, G. Deák, I. Fábián, Z. Csernátony, Synthesis and study of new functionalized silica aerogel poly (methyl methacrylate) composites for biomedical use, Polym. Compos. 36 (2015) 348-358.

[46] M. Gombár, É. Józsa, M. Braun, K. Ősz, Construction of a photochemical reactor combining a CCD spectrophotometer and a LED radiation source, Photochem. Photobiol. Sci. 11 (2012) 1592-1595.

[47] R. Hutter, T. Mallat, A. Baiker, Titania-silica mixed oxides II. Catalytic behaviour in olefin epoxidation, J. Catal. 153 (1995) 177-189.

[48] M. Schraml-Marth, K. L. Walther, A. Wokaun, B. E. Handy, A. Baiker, Porous silica gels and $TiO_2/SiO_2$ mixed oxides prepared via the sol-gel process: characterization by spectroscopic techniques, J. Non-Cryst. Solids 143 (1992) 93-111.

[49] A. Keshavaraja, V. Ramaswamy, H. S. Soni, A. V. Ramaswamy, P. Ratnasamy, Synthesis, characterization and catalytic properties of-micro-mesoporous, amorphous titanosilicate catalysts, J. Catal. 157 (1995) 501-511.

[50] B. Mazinani, A. K. Masrom, A. Beitollahi, R. Luque, Photocatalytic ativity, surface area and phase modification of mesoporous $SiO_2$-$TiO_2$ prepared by one-step hydrothermal procedure, Ceram. Int. 40 (2014) 11525-11532.

[51] R. López, R. Gómez, R. López, R. Gómez, Band-gap energy estimation from diffuse reflectance measurements on sol–gel and commercial $TiO_2$: a comparative study, J. Sol-Gel Sci. Technol. 61 (2012) 1-7.

[52] L. E. Brus, A simple model for the ionization potential, electron affinity, and aqueous redox potentials of small semiconductor crystallites, J. Chem. Phys. 79 (1983) 5566-5571.

[53] G. Lente, J. H. Espenson, Photoreduction of 2,6-Dichloroquinone in aqueous solution. Use of a diode array spectrophotometer concurrently to drive and detect a photochemical reaction, J. Photochem. Photobiol. A 163 (2004) 249-258.

[54] T. Lehóczki, É. Józsa, K. Ősz, Ferroxalate actinometry with online spectrophotometric detection, J. Photochem. Photobiol. A 251 (2013) 63-68.

[55] K. Brodzik, J. Walendziewski, M. Stolarski, L. Van Ginneken, K. Elst, V. Meynen, The influence of preparation method on the physicochemical properties of titania–silica aerogels: Part two, J. Porous Mater. 15 (2008) 541-549.

[56] S. Cao, K. L. Yeung, P. L. Yue, An investigation of trichloroethylene photocatalytic oxidation on mesoporous titania-silica aerogel catalysts, Appl. Catal. B: Environ. 76 (2007) 64-72.

[57] J. Kalmár, É. Dóka, G. Lente, I. Fábián, Aqueous photochemical reactions of chloride, bromide, and iodide ions in a diode-array spectrophotometer. Autoinhibition in the photolysis of iodide ion, Dalton Trans. 43 (2014) 4862-4870.

[58] M. Antonopoulou, D. Vlastos, I. Konstantinou, Photocatalytic degradation of pentachlorophenol by N–F–$TiO_2$: identification of intermediates, mechanism involved, genotoxicity and ecotoxicity evaluation, Photochem. Photobiol. Sci. 14 (2015) 520-524.